

One-Dimensional Luminous Nanorods Featuring Tunable Persistent Luminescence for Autofluorescence-Free Biosensing

Jie Wang,[†] Qinqin Ma,[†] Wei Zheng,[‡] Haoyang Liu,[†] Changqing Yin,[§] Fubing Wang,[§] Xueyuan Chen,[‡] Quan Yuan,^{*,†} and Weihong Tan¹

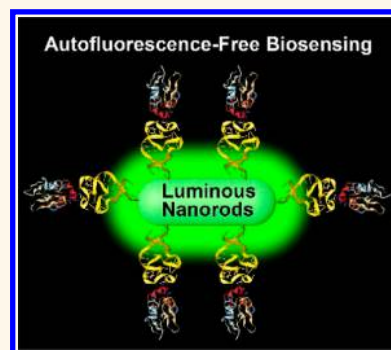
[†]Key Laboratory of Analytical Chemistry for Biology and Medicine (Ministry of Education), College of Chemistry and Molecular Sciences and [§]Department of Laboratory Medicine and Center for Gene Diagnosis, Zhongnan Hospital, Wuhan University, Wuhan 430072, China

[‡]CAS Key Laboratory of Design and Assembly of Functional Nanostructures, Fujian Institute of Research on the Structure of Matter, Chinese Academy of Sciences, Fuzhou, Fujian 350002, China

¹Molecular Science and Biomedicine Laboratory, State Key Laboratory of Chemo/Biosensing and Chemometrics, College of Chemistry and Chemical Engineering, Hunan University, Changsha 410082, China

Supporting Information

ABSTRACT: Persistent luminescence nanoparticles (PLNPs), which can remain luminescent after cessation of excitation, have emerged as important materials in biomedicine due to their special ability to eliminate tissue autofluorescence. Even though significant advances have been made in bioimaging, studies on controlled synthesis of PLNPs with tunable properties are lacking. Until now, only a few studies have reported the synthesis of quasi-spherical $\text{ZnGa}_2\text{O}_4\text{:Cr}$ PLNPs, and direct synthesis of PLNPs with other shapes and chemical compositions has not been reported. Herein, we report the direct synthesis of $\text{Zn}_2\text{GeO}_4\text{:Mn}$ (ZGO:Mn) persistent luminescence nanorods (NRs). The length and persistent luminescence of ZGO:Mn NRs can be fine-tuned by simply changing the pH of the hydrothermal reaction system. Moreover, ZGO:Mn NRs exhibit rapid growth rate, and NRs with strong persistent luminescence can be obtained within 30 min of hydrothermal treatment. Aptamer-guided ZGO:Mn bioprobes were further constructed and applied to serum lysozyme analysis. Serum samples from patients with lung cancer, gastric cancer, and colorectal cancer were collected, and the concentrations of lysozyme in these samples were determined. Since the bioprobes displayed long persistent luminescence, serum autofluorescence interference was completely eliminated. The lysozyme quantification results were in good agreement with those obtained using a clinical method, suggesting the good potential of the bioprobes in the analysis of clinical samples. The developed ZGO:Mn NRs possess tunable length and persistent luminescence, and they are ideal for eliminating autofluorescence interference in biosensing, making them valuable in research areas such as studying the functions of biomolecules and monitoring of molecular/cellular networks in their native contexts.



KEYWORDS: aptamer, autofluorescence, biosensing, persistent luminescence, serum, lysozyme

Persistent luminescence refers to the phenomenon whereby luminescence remains after excitation ceases.^{1–4} Persistent phosphors can store excitation energy in intrinsic traps in the forms of holes or electrons and further release the trapped charge carriers to produce photonic emission under thermal or other stimulation.^{5–10} The past years have witnessed the widespread usage of persistent luminescence nanoparticles (designated as PLNPs) in biomedicine,^{11–14} especially in bioimaging.^{15–18} Since *in situ* excitation is not involved,^{19–21} PLNPs can efficiently eliminate tissue autofluorescence and light scattering interference in bioimaging, leading to significant improvement of imaging sensitivity and signal-to-noise ratio.^{22–24} Moreover, PLNPs are

suitable for long-term bioimaging due to their long-lasting luminescence.^{25–27} While considerable achievements in bioimaging have been made, study of the controlled synthesis of PLNPs remains largely unexplored, even though there are growing demands for PLNPs with tunable properties in biomedicine. At present, most of the PLNPs are prepared by a “top-down” method, in which high-temperature annealing is involved, which produces particles with uneven size that cannot

Received: May 5, 2017

Accepted: June 30, 2017

Published: June 30, 2017

be dispersed in water.² Recently, Han and other research groups reported the direct synthesis of PLNPs *via* a “bottom-up” manner.^{28–31} However, all of these studies were restricted to the synthesis of quasi-spherical $\text{ZnGa}_2\text{O}_4\cdot\text{Cr}^{3+}$ nanoparticles. Direct synthesis of PLNPs with other shapes and chemical compositions has not been reported. Furthermore, the biomedical applications of PLNPs are usually restricted to bioimaging, while usage of PLNPs in other areas remains largely unexplored.

According to the periodic bond chain theory, nanomaterials with phenacite structure prefer to grow in the direction of the *c*-axis and form nanorods or nanowires, since planes horizontal to the *c*-axis such as (110) are energetically more stable than (001).^{32,33} Zn_2GeO_4 shows typical phenacite structure,^{34–36} and several researchers have observed persistent luminescence in Zn_2GeO_4 -based bulk phosphors.^{37–40} Therefore, Zn_2GeO_4 can serve as a potential host material for the synthesis of PLNPs.

Herein, we report the direct hydrothermal synthesis of $\text{Zn}_2\text{GeO}_4\text{:Mn}$ (designated as ZGO:Mn) persistent nanorods (NRs) with tunable properties. The length, persistent luminescence intensity, and decay time of ZGO:Mn NRs can be fine-tuned by simply changing the pH of the hydrothermal reaction system. The application of the ZGO:Mn NRs in autofluorescence-free biosensing was further investigated. Aptamer-guided ZGO:Mn biosensing probes were constructed for lysozyme detection in serum of cancer patients. Blood samples from patients with lung cancer, gastric cancer, and colorectal cancer were collected, and the corresponding serum samples were further prepared. The biosensing probes were used to measure lysozyme concentrations in the serum samples without *in situ* excitation. The autofluorescence interference from serum was efficiently eliminated by the probes due to the long persistent luminescence. Moreover, the lysozyme detection results were in good agreement with those obtained using clinical ELISA, which indicated that the biosensing probes were highly reliable for analysis of clinical samples. These ZGO:Mn NRs exhibit highly tunable properties and show good promise in clinical analyses as well as in studies of the role of biomolecules in their native contexts.

RESULTS AND DISCUSSION

The shape and crystal structure of ZGO:Mn PLNPs prepared at different pHs were characterized with transmission electron microscopy (TEM) and X-ray powder diffraction (XRD). As shown in Figure 1 and Figure S1, all of the ZGO:Mn display typical rod shape and are well-dispersed. With increasing pH from 6 to 7.5 (Figure 1a–d), the length of the ZGO:Mn NRs decreased rapidly from about 900 nm to about 60 nm. Further increase in pH to 9.5 (Figure 1d–f) led to a slight increase of the length to about 80 nm. The XRD pattern of ZGO:Mn NRs can be assigned to the rhombohedral phase of Zn_2GeO_4 (Figure S2).^{35,40} High-resolution TEM (HRTEM) images (Figure 1g–l) show well-resolved lattice fringes, indicating that all the ZGO:Mn NRs are highly crystalline. Detailed crystal structure of the ZGO:Mn NRs was further studied with high-resolution high-angle annular dark-field scanning transmission electron microscopy (HAADF-STEM). Spacing of 0.71 nm (110) between the adjacent lattice fringes is observed parallel to the rod direction, and another lattice fringe of (113) with an interplanar spacing of 0.29 nm is also observed at an angle of 66° to the rod direction (Figure S3),⁴¹ indicating that the ZGO:Mn NRs grow in the direction of the *c*-axis. Energy-

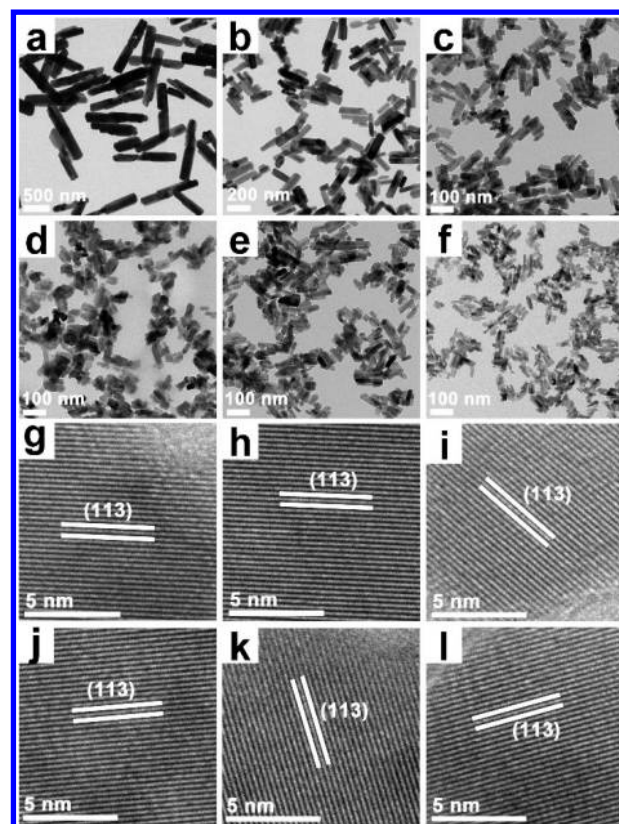


Figure 1. TEM (a–f) and HRTEM (g–l) images of the ZGO:Mn NRs prepared at different pH values (a and g, pH = 6.0; b and h, pH = 6.5; c and i, pH = 7.0; d and j, pH = 7.5; e and k, pH = 8.5; f and l, pH = 9.5).

dispersive X-ray analysis further shows the presence of Mn in the developed NRs (Figure S4). The above results clearly show that ZGO:Mn NRs with tunable length were successfully prepared by our hydrothermal method.

The luminescence properties of ZGO:Mn NRs were further investigated. Figure 2a presents the photoluminescence spectrum of ZGO:Mn NRs. The emission bands peaking at around 450 and 480 nm can be attributed to intrinsic defects such as oxygen vacancies and interstitial Zn.⁴² For ZGO:Mn NRs prepared at pH below 7.0, the emission of Mn^{2+} at around 536 nm is seriously overlapped by the defect luminescence. With increasing pH, the defect luminescence gradually weakens, and a strong emission band from Mn^{2+} is observed. The defect luminescence nearly disappears, and green emission dominates the spectrum at pH = 9.5. The quantum yields of ZGO:Mn NRs prepared at different pHs were measured and presented in Table S1. The persistent luminescence decay in ZGO:Mn NRs was further measured, as shown in Figure 2b. Obviously, all of the ZGO:Mn NRs exhibit distinct persistent luminescence with decay times longer than 100 s, clearly demonstrating the successful preparation of ZGO:Mn persistent NRs. Moreover, the persistent luminescence intensity and decay time can be tuned by simply changing the pH. Figure 2c and Figure S5a present the photoluminescence images of ZGO:Mn NRs dispersions. The color of the dispersions gradually changes from blue to green with increasing pH, which can be attributed to the gradual decrease of defect luminescence and increase of Mn^{2+} emission. The persistent luminescence images were further captured with a commercial camera after cessation of excitation. As shown in Figure 2d and

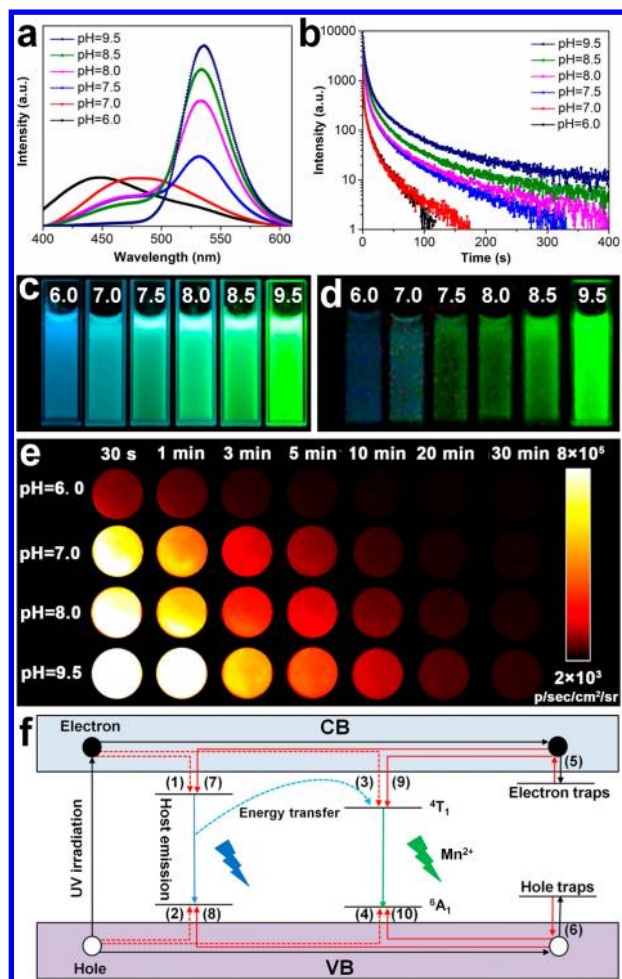


Figure 2. Photoluminescence spectra (a) and persistent luminescence decay (b) of the ZGO:Mn NRs. Photoluminescence (c) and persistent luminescence (d) images of the ZGO:Mn NRs. (e) Persistent luminescence decay images of the ZGO:Mn NRs. (f) Schematic illustration about the mechanism of persistent luminescence in ZGO:Mn NRs.

Figure S5b, all of the prepared ZGO:Mn NRs display strong persistent luminescence, and tuning of the persistent luminescence color is also observed. The persistent luminescence of ZGO:Mn NRs was further measured with an IVIS Lumina XR imaging system, as shown in Figure 2e. Strong persistent luminescence is observed in all of the ZGO:Mn NRs, and the decay time can be tuned from 3 min to more than 30 min. The mechanism of persistent luminescence in ZGO:Mn NRs is illustrated in Figure 2f.^{43,44} The excited electrons and holes generated under UV excitation are captured by the electron and hole traps, respectively (7). Under thermal stimulation, some of the trapped charge carriers can escape from the traps and move to the native defects, leading to the generation of host emission (8). Also, some of the escaped electrons can move to the excited energy level of Mn^{2+} (9), and the combination of the electrons with holes results in the green emission from Mn^{2+} (6). All of the above results clearly demonstrate the successful development of ZGO:Mn persistent luminescence NRs. Moreover, the length and persistent luminescence in the NRs can be fine-tuned by simply changing the pH of the hydrothermal reaction system.

In addition to tunable size and persistent luminescence, rapid growth rate of ZGO:Mn NRs was also observed. The growth of

ZGO:Mn NRs at pH = 9.5 was systematically characterized. The reaction solution containing Zn, Ge, and Mn precursors was first stirred at room temperature. As shown in Figure 3a

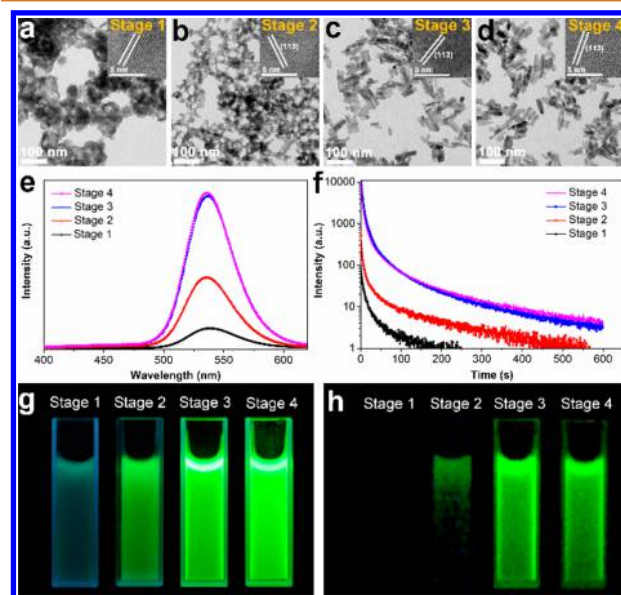


Figure 3. (a–d) TEM images of nanoparticles obtained from different reaction stages in the preparation of ZGO:Mn NRs at pH = 9.5 (Stages 1 and 2, nanoparticles obtained after 30 and 60 min of stirring at room temperature, respectively; stages 3 and 4, NRs obtained after 30 min and 4 h of hydrothermal treatment, respectively). Photoluminescence spectra (e) and persistent luminescence decay (f) of nanoparticles obtained from the above four stages. Photoluminescence (g) and persistent luminescence (h) images of nanoparticles obtained from the above four stages.

and Figure S12, wrinkled nanoparticles were formed after 30 min (Stage 1), and the XRD pattern indicates the rhombohedral structure of the nanoparticles (Figure S13). The wrinkled nanoparticles gradually merged after 60 min of stirring (Figure 3b, Stage 2). The reaction solution was then subjected to thermal treatment at 220 °C. Figure 3c shows that highly crystallized ZGO:Mn NRs were obtained after 30 min of hydrothermal treatment (Stage 3), and further increase in the reaction time to 4 h did not lead to obvious morphological or crystallinity changes (Figure 3d, Stage 4, and Figure S12). The luminescence properties of particles obtained at the above four stages were further studied. Figure 3e presents the photoluminescence spectra of the particles. Typical green emission is observed in nanoparticles from all of the four stages. Figure 3f shows that nanoparticles obtained at room temperature (Stages 1 and 2) already display obvious persistent luminescence. Moreover, ZGO:Mn NRs at Stage 3 display a decay curve similar to that of NRs obtained at Stage 4, clearly indicating that ZGO:Mn NRs can be prepared within 30 min of hydrothermal treatment. The photoluminescence and persistent luminescence images of the above particle dispersions were further captured with a commercial camera. As shown in Figure 3g, green luminescence is observed in nanoparticles obtained at room temperature (Stages 1 and 2), and the ZGO:Mn NRs (Stages 3 and 4) exhibit bright green luminescence. Figure 3h further shows the strong persistent luminescence of the ZGO:Mn NRs. The above results thus clearly suggest that NRs with strong persistent luminescence can be easily obtained

within 30 min of hydrothermal treatment, indicating the rapid growth rates of ZGO:Mn NRs.

The ZGO:Mn NRs were further employed for autofluorescence-free biosensing. Because previous studies reported that the abnormal expression of serum lysozyme is highly correlated with solid tumors,^{45–47} lysozyme was utilized as the model target in our study. The detection of lysozyme in serum is illustrated in Figure 4a. The ZGO:Mn NRs were functionalized

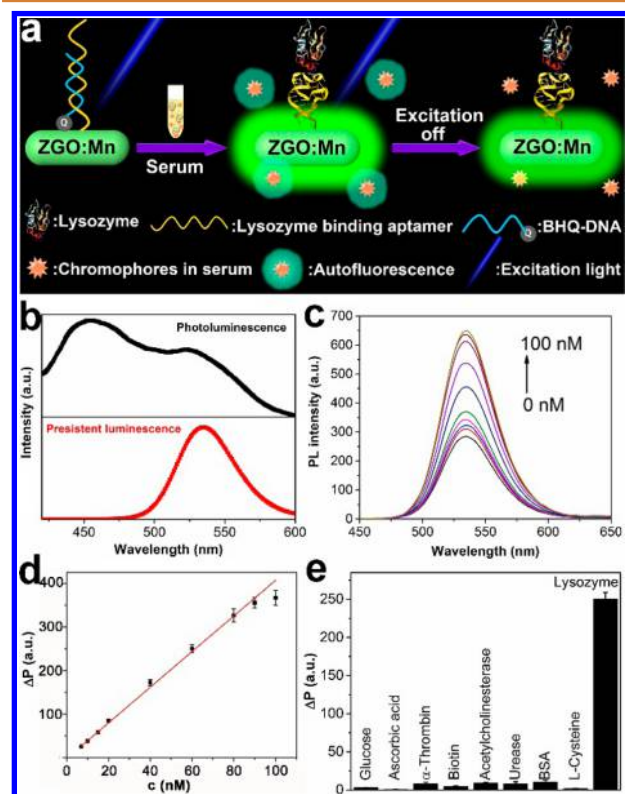


Figure 4. (a) Schematic illustration of autofluorescence-free serum lysozyme biosensing. (b) Photoluminescence and persistent luminescence spectra of human serum containing ZGO:Mn-LBA. (c) Recovery of persistent luminescence in the presence of lysozyme with different concentrations. (d) Plot of enhanced persistent luminescence intensity (ΔP) versus lysozyme concentration. (e) Responses of the biosensing probes to different kinds of biomolecules.

with lysozyme-binding aptamer^{48,49} (designated as ZGO:Mn-LBA), and black-hole-quencher-labeled DNA (designated as BHQ-DNA) was used to quench the luminescence of ZGO:Mn-LBA through DNA hybridization. The aptamer folds into a unique 3D structure, which binds with lysozyme and the BHQ-DNA is detached from the ZGO:Mn-LBA. As a result, the luminescence of ZGO:Mn-LBA is recovered. The biological chromophores in serum display strong autofluorescence under excitation, causing serious interferences with the traditional fluorescence assay. However, in this study, the short-lived autofluorescence decays rapidly after excitation ceases, but the ZGO:Mn-LBA remains luminescent. By collecting the persistent luminescence signal of ZGO:Mn-LBA, the autofluorescence interference from serum can be efficiently eliminated. TEM images show that LBA modification did not cause any obvious changes to the shapes or dispersibility of the ZGO:Mn NRs (Figure S14). The successful preparation of ZGO:Mn-LBA bioprobe was evidenced by zeta potential

measurement (Figure S15). To test the effectiveness of ZGO:Mn-LBA in suppression of autofluorescence, human serum was added to the ZGO:Mn-LBA dispersion. The photoluminescence and persistent luminescence spectra of the solution were measured and are presented in Figure 4b. The photoluminescence curve shows that human serum exhibits strong fluorescence in the range of 400–600 nm, and the autofluorescence seriously blurs the emission band of ZGO:Mn-LBA at 536 nm. However, upon removal of the excitation source, serum autofluorescence disappears completely, and the distinct emission band of ZGO:Mn-LBA is obtained, as evidenced by the persistent luminescence curve in Figure 4b. These results clearly demonstrate that ZGO:Mn-LBA can efficiently eliminate serum autofluorescence interference. The response of the biosensing probe to lysozyme was further tested. As shown in Figure 4c, addition of lysozyme leads to efficient recovery of the persistent luminescence, indicating the efficient displacement of BHQ-DNA by lysozyme. A good linear relationship between the enhanced persistent luminescence (ΔP) and the concentration of added lysozyme is observed (Figure 4d). The detection limit of lysozyme was 4.6 nM estimated using 3σ . The specificity of the biosensing probe was further tested, and the results are presented in Figure 4e. High specificity toward lysozyme is observed, which can be attributed to the specific binding affinity of aptamers to their targets.^{50,51}

The biosensing probe was further utilized to detect lysozyme in serum from cancer patients. As illustrated in Figure 5a, blood

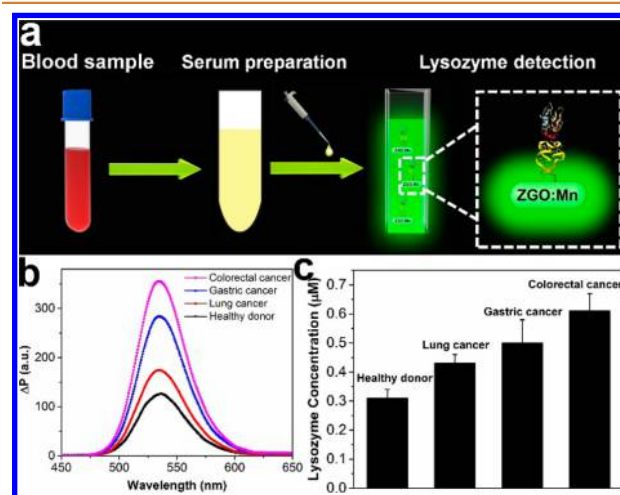


Figure 5. (a) Schematic illustration of the preparation of serum samples from cancer patients. (b) Response of the biosensing probes to different kinds of serum samples. (c) Concentrations of lysozyme in different kinds of serum determined with the biosensing probes.

samples were collected from cancer patients, and serum samples were prepared by removing cells from the blood *via* centrifugation. Serum sample from patients with lung cancer, gastric cancer, and colorectal cancer were tested. For comparison, serum samples from healthy volunteers were also tested. As shown in Figure 5b, serum from healthy donors leads to obvious enhancement of the luminescence signal, suggesting the presence of lysozyme in the serum of healthy donors. As for serum from cancer patients, a larger enhancement of emission intensity is observed, indicating the increased amounts of lysozyme in serum from cancer patients. The concentrations of

lysozyme in different serum samples are further presented in Figure 5c. The overexpression of serum lysozyme is clearly observed in cancer patients. To confirm the above detection results, the lysozyme concentrations in serum samples were in parallel determined by clinical ELISA. As shown in Table 1, the

Table 1. Results of Lysozyme Concentrations in Different Kinds of Serum Samples Determined with ZGO:Mn-LBA Biosensing Probes and ELISA, Respectively

serum	method	concentration (μM)
healthy donor	ZGO:Mn-LBA	0.31 ± 0.03
lung cancer	ZGO:Mn-LBA	0.43 ± 0.03
gastric cancer	ZGO:Mn-LBA	0.50 ± 0.08
colorectal cancer	ZGO:Mn-LBA	0.61 ± 0.06
healthy donor	ELISA	0.33 ± 0.05
lung cancer	ELISA	0.41 ± 0.06
gastric cancer	ELISA	0.47 ± 0.05
colorectal cancer	ELISA	0.56 ± 0.08

results obtained with the ZGO:Mn-LBA probe are in good agreement with those obtained using ELISA. These results thus suggest that the ZGO:Mn-LBA biosensing probe is highly reliable in the analysis of clinical samples.

CONCLUSIONS

In this work, we have highlighted the direct synthesis of ZGO:Mn persistent luminescence NRs. Both the length and persistent luminescence of ZGO:Mn NRs can be fine-tuned by simply changing the pH of the hydrothermal reaction system. Additionally, the ZGO:Mn exhibits rapid growth rate, and NRs with strong persistent luminescence can be obtained within 30 min of hydrothermal treatment. Because ZGO:Mn can remain luminescent for tens of minutes, autofluorescence from biological samples was efficiently eliminated. Lysozyme binding aptamer guided ZGO:Mn NRs were employed for lysozyme detection in serum from cancer patients, and the detection results were in good agreement with those obtained using clinical ELISA. To conclude, ZGO:Mn persistent luminescence NRs with tunable length and persistent luminescence were successfully developed. The ZGO:Mn NRs exhibit good performance in biosensing, which makes them valuable in studying the biological functions of biomolecules and monitoring cellular networks in their native contexts.

EXPERIMENTAL SECTION

Preparation of the $\text{Zn}_2\text{GeO}_4\text{:Mn}$ (ZGO:Mn) Nanorods. The ZGO:Mn nanorods were synthesized by a hydrothermal method. Briefly, 2 mmol of $\text{Zn}(\text{NO}_3)_2$, 0.005 mmol of $\text{Mn}(\text{NO}_3)_2$, and 300 μL of concentrated HNO_3 were added into 11 mL of deionized water under vigorous stirring. Then, 1 mmol of Na_2GeO_3 was slowly added to the above solution. After that, ammonium hydroxide (28%, wt) was immediately added to adjust the pH of the solution to the desired value. The resultant reaction system was left at room temperature for 1 h with stirring. Then the solution was transferred to a Teflon-lined autoclave and allowed to react at 220 $^\circ\text{C}$ for 4 h. The resultant ZGO:Mn nanorods were collected by centrifugation and were washed three times with deionized water.

Measurement of the Decay Images of ZGO:Mn Nanorods. The ZGO:Mn nanorods (0.1 g) prepared at different pHs were placed into a 48-well plate. The nanorods were illuminated with a portable UV lamp for 3 min. After that, the UV lamp was removed, and the plate was immediately put into the IVIS Lumina XR Imaging System to record the decay images.

Preparation of Aptamer-Guided ZGO:Mn. The ZGO:Mn nanorods were first functionalized with amino groups (designated as ZGO:Mn-NH₂). Typically, 25 mg of ZGO:Mn nanorods were dispersed in 10 mL of DMF with sonication. Then APTES (100 μL) was dropwise added into the above solution under vigorous stirring. The resultant solution was allowed to react at 80 $^\circ\text{C}$ for 12 h. The as-prepared ZGO:Mn-NH₂ nanorods were washed with DMF and further dispersed in 15 mL of deionized water. The preparation of aptamer-guided ZGO:Mn was further conducted with a previously reported protocol.⁵² The preparation of ZGO:Mn-LBA is used as an example. Briefly, ZGO:Mn-NH₂ nanorods (1 mg) and Sulfo-SMCC (0.2 mg) were added to 1 mL of HEPES buffer (10 mM, pH = 7.2). The solution was kept at 25 $^\circ\text{C}$ for 30 min with shaking. The maleimide-activated ZGO:Mn-NH₂ nanorods were collected by centrifugation, and excess Sulfo-SMCC was removed by washing several times with Tris-HCl buffer (10 mM, pH = 7.4). After that, the activated ZGO:Mn-NH₂ nanorods were redispersed in 1 mL of Tris-HCl buffer containing 2 nmol lysozyme-binding aptamer. The solution was incubated at 25 $^\circ\text{C}$ for 12 h. Then the resultant ZGO:Mn-LBA was collected by centrifugation and was redispersed in 1 mL of Tris-HCl buffer for further use.

Detection of Lysozyme in Tris-HCl Buffer. The ZGO:Mn-LBA (1 mg) was incubated with 1 nmol of BHQ-DNA at 37 $^\circ\text{C}$ for 12 h under shaking. Then the biosensing probes were collected by centrifugation and further dispersed in 1 mL of Tris-HCl buffer after washing with buffer to remove free BHQ-DNA. For the detection of lysozyme, 100 μL of the bioprobes was added into 300 μL of lysozyme solution. The biosensing system was incubated at 37 $^\circ\text{C}$ for 4 h. After that, the persistent luminescence intensity of the biosensing system was measured on a fluorescence spectrometer without *in situ* excitation.

Detection of Lysozyme in Serum from Cancer Patients. Typically, 40 μL of serum and 100 μL of the bioprobes solution were added into 260 μL of Tris-HCl buffer. The biosensing system was incubated at 37 $^\circ\text{C}$ for 4 h. Then the persistent luminescence intensity of the biosensing system was measured without *in situ* excitation.

ASSOCIATED CONTENT

Supporting Information

The Supporting Information is available free of charge on the ACS Publications website at DOI: 10.1021/acsnano.7b03128.

TEM images and XRD patterns of ZGO:Mn NRs prepared at different pHs, HAADF-STEM images and EDX analysis of the ZGO:Mn NRs, photoluminescence and persistent luminescence images of ZGO:Mn nanorods, TEM and XRD characterization of the growth of ZGO:Mn nanorods, TEM images of ZGO:Mn-LBA, zeta potentials of ZGO:Mn, ZGO:Mn-NH₂, ZGO:Mn-LBA (PDF)

AUTHOR INFORMATION

Corresponding Author

*E-mail: yuanquan@whu.edu.cn.

ORCID

Xueyuan Chen: 0000-0003-0493-839X

Quan Yuan: 0000-0002-3085-431X

Weihong Tan: 0000-0002-8066-1524

Notes

The authors declare no competing financial interest.

ACKNOWLEDGMENTS

This work was supported by the National Natural Science Foundation of China (21422105, 21675120, 21325104) and the CAS/SAFEA International Partnership Program for

Creative Research Teams. Q.Y. thanks the large-scale instrument and equipment sharing foundation of Wuhan University.

REFERENCES

- (1) Matsuzawa, T.; Aoki, Y.; Takeuchi, N.; Murayama, Y. A New Long Phosphorescent Phosphor with High Brightness, $\text{SrAl}_2\text{O}_4:\text{Eu}^{2+}, \text{Dy}^{3+}$. *J. Electrochem. Soc.* **1996**, *143*, 2670–2673.
- (2) Li, Y.; Gecevicius, M.; Qiu, J. Long Persistent Phosphors—from Fundamentals to Applications. *Chem. Soc. Rev.* **2016**, *45*, 2090–2136.
- (3) Pan, Z.; Lu, Y. Y.; Liu, F. Sunlight-Activated Long-Persistent Luminescence in the Near-Infrared from Cr^{3+} -Doped Zinc Gallogermanates. *Nat. Mater.* **2012**, *11*, 58–63.
- (4) Wang, J.; Ma, Q. Q.; Wang, Y. Q.; Shen, H. J.; Yuan, Q. Recent Progress in Biomedical Applications of Persistent Luminescence Nanoparticles. *Nanoscale* **2017**, *9*, 6204–6218.
- (5) Zhou, Z. Z.; Zheng, W.; Kong, J. T.; Liu, Y.; Huang, P.; Zhou, S. Y.; Chen, Z.; Shi, J. L.; Chen, X. Y. Rechargeable and LED-Activated $\text{ZnGa}_2\text{O}_4:\text{Cr}^{3+}$ Near-Infrared Persistent Luminescence Nanoprobes for Background-Free Biodetection. *Nanoscale* **2017**, *9*, 6846–6853.
- (6) Zou, R.; Huang, J. J.; Shi, J. P.; Huang, L.; Zhang, X. J.; Wong, K. L.; Zhang, H. W.; Jin, D. Y.; Wang, J.; Su, Q. Silica Shell-Assisted Synthetic Route for Mono-disperse Persistent Nanophosphors with Enhanced *in Vivo* Recharged Near-Infrared Persistent Luminescence. *Nano Res.* **2017**, *10*, 2070–2082.
- (7) Zou, Z.; Lin, F.; Cao, C.; Zhang, J.; Wang, Y. Near-Infrared Quantum Cutting Long Persistent Luminescence. *Sci. Rep.* **2016**, *6*, 24884.
- (8) Kong, J.; Zheng, W.; Liu, Y.; Li, R.; Ma, E.; Zhu, H.; Chen, X. Persistent Luminescence from Eu^{3+} in SnO_2 Nanoparticles. *Nanoscale* **2015**, *7*, 11048–11054.
- (9) Song, L.; Lin, X. H.; Song, X. R.; Chen, S.; Chen, X. F.; Li, J.; Yang, H. H. Repeatable Deep-Tissue Activation of Persistent Luminescent Nanoparticles by Soft X-Ray for High Sensitivity Long-Term *in Vivo* Bioimaging. *Nanoscale* **2017**, *9*, 2718–2722.
- (10) Li, Y.; Chen, R.; Sharafudeen, K.; Zhou, S.; Gecevicius, M.; Wang, H.; Dong, G.; Wu, Y.; Qin, X.; Qiu, J. Tailoring of the Trap Distribution and Crystal Field in Cr^{3+} -Doped Non-Gallate Phosphors with Near-Infrared Long-Persistence Phosphorescence. *NPG Asia Mater.* **2015**, *7*, e180.
- (11) Wu, B. Y.; Wang, H. F.; Chen, J. T.; Yan, X. P. Fluorescence Resonance Energy Transfer Inhibition Assay for α -Fetoprotein Excreted during Cancer Cell Growth Using Functionalized Persistent Luminescence Nanoparticles. *J. Am. Chem. Soc.* **2011**, *133*, 686–688.
- (12) Li, N.; Li, Y. H.; Han, Y. Y.; Pan, W.; Zhang, T. T.; Tang, B. A Highly Selective and Instantaneous Nanoprobe for Detection and Imaging of Ascorbic Acid in Living Cells and *in Vivo*. *Anal. Chem.* **2014**, *86*, 3924–3930.
- (13) Maldiney, T.; Bessière, A.; Seguin, J.; Teston, E.; Sharma, S. K.; Viana, B.; Bos, A. J.; Dorenbos, P.; Bessodes, M.; Gourier, D.; et al. The *in Vivo* Activation of Persistent Nanophosphors for Optical Imaging of Vascularization, Tumours and Grafted Cells. *Nat. Mater.* **2014**, *13*, 418–426.
- (14) Li, N.; Diao, W.; Han, Y.; Pan, W.; Zhang, T.; Tang, B. MnO_2 -Modified Persistent Luminescence Nanoparticles for Detection and Imaging of Glutathione in Living Cells and *in Vivo*. *Chem. - Eur. J.* **2014**, *20*, 16488–16491.
- (15) Li, Z. J.; Zhang, H. W.; Sun, M.; Shen, J. S.; Fu, H. X. A Facile and Effective Method to Prepare Long-Persistent Phosphorescent Nanospheres and Its Potential Application for *in Vivo* Imaging. *J. Mater. Chem.* **2012**, *22*, 24713–24720.
- (16) Shi, J.; Sun, X.; Li, J.; Man, H.; Shen, J.; Yu, Y.; Zhang, H. Multifunctional Near Infrared-Emitting Long-Persistent Phosphorescent Nanospheres for Drug Delivery and Targeted Tumor Imaging. *Biomaterials* **2015**, *37*, 260–270.
- (17) Zhang, L.; Lei, J.; Liu, J.; Ma, F.; Ju, H. Persistent Luminescence Nanoprobe for Biosensing and Lifetime Imaging of Cell Apoptosis *via* Time-Resolved Fluorescence Resonance Energy Transfer. *Biomaterials* **2015**, *67*, 323–334.
- (18) Singh, S. K. Red and Near Infrared Persistent Luminescence Nano-Probes for Bioimaging and Targeting Applications. *RSC Adv.* **2014**, *4*, 58674–58698.
- (19) Abdulkayum, A.; Yang, C. X.; Zhao, Q.; Chen, J. T.; Dong, L. X.; Yan, X. P. Gadolinium Complexes Functionalized Persistent Luminescent Nanoparticles as a Multimodal Probe for Near-Infrared Luminescence and Magnetic Resonance Imaging *in Vivo*. *Anal. Chem.* **2014**, *86*, 4096–4101.
- (20) Sun, M.; Li, Z. J.; Liu, C. L.; Fu, H. X.; Shen, J. S.; Zhang, H. W. Persistent Luminescent Nanoparticles for Super-Long Time *in Vivo* and *in Situ* Imaging with Repeatable Excitation. *J. Lumin.* **2014**, *145*, 838–843.
- (21) Li, Y. J.; Yan, X. P. Synthesis of Functionalized Triple-Doped Zinc Gallogermanate Nanoparticles with Superlong Near-Infrared Persistent Luminescence for Long-Term Orally Administrated Bioimaging. *Nanoscale* **2016**, *8*, 14965–14970.
- (22) Abdulkayum, A.; Chen, J. T.; Zhao, Q.; Yan, X. P. Functional Near Infrared-Emitting $\text{Cr}^{3+}/\text{Pr}^{3+}$ Co-Doped Zinc Gallogermanate Persistent Luminescent Nanoparticles with Superlong Afterglow for *in Vivo* Targeted Bioimaging. *J. Am. Chem. Soc.* **2013**, *135*, 14125–14133.
- (23) Li, Z.; Zhang, Y.; Wu, X.; Maudgal, R.; Zhang, H.; Han, G. *In Vivo* Repeatedly Charging Near-Infrared-Emitting Mesoporous $\text{SiO}_2/\text{ZnGa}_2\text{O}_4:\text{Cr}^{3+}$ Persistent Luminescence Nanocomposites. *Adv. Sci.* **2015**, *2*, 1500001.
- (24) de Chermont, Q. I. M.; Chanéac, C.; Seguin, J.; Pellé, F.; Maitrejean, S.; Jolivet, J. P.; Gourier, D.; Bessodes, M.; Scherman, D. Nanoprobes with Near-Infrared Persistent Luminescence for *in Vivo* Imaging. *Proc. Natl. Acad. Sci. U. S. A.* **2007**, *104*, 9266–9271.
- (25) Fu, X.; Liu, C.; Shi, J.; Man, H.; Xu, J.; Zhang, H. Long Persistent Near Infrared Luminescence Nanoprobes $\text{LiGa}_2\text{O}_8:\text{Cr}^{3+}$ -PEG-OCH₃ for *in Vivo* Imaging. *Opt. Mater.* **2014**, *36*, 1792–1797.
- (26) Wu, S. Q.; Chi, C. W.; Yang, C. X.; Yan, X. P. Penetrating Peptide-Bioconjugated Persistent Nanophosphors for Long-Term Tracking of Adipose-Derived Stem Cells with Superior Signal-to-Noise Ratio. *Anal. Chem.* **2016**, *88*, 4114–4121.
- (27) Maldiney, T.; Doan, B.; Alloyeau, D.; Bessodes, M.; Scherman, D.; Richard, C. Gadolinium-Doped Persistent Nanophosphors as Versatile Tool for Multimodal *in Vivo* Imaging. *Adv. Funct. Mater.* **2015**, *25*, 331–338.
- (28) Li, Z.; Zhang, Y.; Wu, X.; Huang, L.; Li, D.; Fan, W.; Han, G. Direct Aqueous-Phase Synthesis of Sub-10 nm “Luminous Pearls” with Enhanced *in Vivo* Renewable Near-Infrared Persistent Luminescence. *J. Am. Chem. Soc.* **2015**, *137*, 5304–5307.
- (29) Teston, E.; Richard, S.; Maldiney, T.; Lièvre, N.; Wang, G. Y.; Motte, L.; Richard, C.; Lalatonne, Y. Non-Aqueous Sol-Gel Synthesis of Ultra Small Persistent Luminescence Nanoparticles for Near-Infrared *in Vivo* Imaging. *Chem. - Eur. J.* **2015**, *21*, 7350–7354.
- (30) Shi, J.; Sun, X.; Zhu, J.; Li, J.; Zhang, H. One-Tstep Synthesis of Amino-Functionalized Ultrasmall Near Infrared-Emitting Persistent Luminescent Nanoparticles for *in Vitro* and *in Vivo* Bioimaging. *Nanoscale* **2016**, *8*, 9798–9804.
- (31) Srivastava, B. B.; Kuang, A.; Mao, Y. Persistent Luminescent Sub-10 nm Cr Doped ZnGa_2O_4 Nanoparticles by a Biphasic Synthesis Route. *Chem. Commun.* **2015**, *51*, 7372–7375.
- (32) Hartman, P.; Perdok, W. G. On the Relations between Structure and Morphology of Crystals. I. *Acta Crystallogr.* **1955**, *8*, 49–52.
- (33) Sun, C.; Kuan, C.; Kao, F. J.; Wang, Y. M.; Chen, J. C.; Chang, C. C.; Shen, P. On the Nucleation, Growth and Impingement of Plate-Like α - Zn_2SiO_4 Spherulites in Glaze Layer: a Confocal and Electron Microscopic Study. *Mater. Sci. Eng., A* **2004**, *379*, 327–333.
- (34) Yamaguchi, O.; Hidaka, J.; Hirota, K. Formation and Characterization of Alkoxy-Derived Zn_2GeO_4 . *J. Mater. Sci. Lett.* **1991**, *10*, 1471–1474.
- (35) Zou, F.; Hu, X.; Sun, Y.; Luo, W.; Xia, F.; Long, Q.; Jiang, Y.; Huang, Y. Facile Synthesis of Sandwiched Zn_2GeO_4 -Graphene Oxide Nanocomposite as a Stable and High-Capacity Anode for Lithium-Ion Batteries. *Nanoscale* **2014**, *6*, 924–930.
- (36) Stevens, R.; Woodfield, B. F.; Boerio-Goates, J.; Crawford, M. K. Heat Capacities, Third-Law Entropies and Thermodynamic Func-

tions of the Negative Thermal Expansion Material Zn_2GeO_4 from $T = (0 \text{ to } 400) \text{ K}$. *J. Chem. Thermodyn.* **2004**, *36*, 349–357.

(37) Woo, B. K.; Luo, Z.; Li, Y.; Singh, S. P.; Joly, A. G.; Hossu, M.; Liu, Z.; Chen, W. Luminescence Enhancement of $\text{CaZnGe}_2\text{O}_6:\text{Tb}^{3+}$ Afterglow Phosphors Synthesized Using ZnO Nanopowders. *Opt. Mater.* **2011**, *33*, 1283–1290.

(38) Jin, Y.; Hu, Y.; Fu, Y.; Ju, G.; Mu, Z.; Chen, R.; Lin, J.; Wang, Z. Preparation, Design, and Characterization of the Novel Long Persistent Phosphors: $\text{Na}_2\text{ZnGeO}_4$ and $\text{Na}_2\text{ZnGeO}_4:\text{Mn}^{2+}$. *J. Am. Ceram. Soc.* **2015**, *98*, 1555–1561.

(39) Cong, Y.; He, Y.; Dong, B.; Xiao, Y.; Wang, L. Long Afterglow Properties of $\text{Zn}_2\text{GeO}_4:\text{Mn}^{2+}$, Cr^{3+} Phosphor. *Opt. Mater.* **2015**, *42*, 506–510.

(40) Wan, M.; Wang, Y.; Wang, X.; Hui, Z.; Hu, Z. The Properties of a Novel Green Long Afterglow Phosphor $\text{Zn}_2\text{GeO}_4:\text{Mn}^{2+}$, Pr^{3+} . *Opt. Mater.* **2014**, *36*, 650–654.

(41) Mukherjee, B.; Varghese, B.; Zheng, M.; Karthik, K. R. G.; Mathews, N.; Mhaisalkar, S. G.; Tok, E. S.; Sow, C. H. Synthesis, Characterization and Electrical Properties of Hybrid $\text{Zn}_2\text{GeO}_4\text{--ZnO}$ Beaded Nanowire Arrays. *J. Cryst. Growth* **2012**, *346*, 32–39.

(42) Gu, Z.; Liu, F.; Li, X.; Pan, Z. W. Luminescent Zn_2GeO_4 Nanorod Arrays and Nanowires. *Phys. Chem. Chem. Phys.* **2013**, *15*, 7488–7493.

(43) Cong, Y.; He, Y. Y.; Dong, B.; Xiao, Y.; Wang, L. M. Long Afterglow Properties of $\text{Zn}_2\text{GeO}_4:\text{Mn}^{2+}$, Cr^{3+} Phosphor. *Opt. Mater.* **2015**, *42*, 506–510.

(44) Jin, Y. H.; Hu, Y. H.; Duan, H.; Chen, L.; Wang, X. J. The Long Persistent Luminescence Properties of Phosphors: $\text{Li}_2\text{ZnGeO}_4$ and $\text{Li}_2\text{ZnGeO}_4:\text{Mn}^{2+}$. *RSC Adv.* **2014**, *4*, 11360–11366.

(45) Currie, G. Serum Lysozyme as a Marker of Host Resistance. II. Patients with Malignant Melanoma, Hypernephroma or Breast Carcinoma. *Br. J. Cancer* **1976**, *33*, 593–599.

(46) Luger, T.; Kokoschka, E.; Sagaster, P.; Micksche, M. Serum Lysozyme Levels in Patients with Solid Tumors. *Oncology* **1979**, *36*, 15–18.

(47) Yuen, S.; Wong, M.; Chung, L.; Chan, S.; Cheung, N.; Ho, J.; Leung, S. Up-Regulation of Lysozyme Production in Colonic Adenomas and Adenocarcinomas. *Histopathology* **1998**, *32*, 126–132.

(48) Song, Y.; Li, Y.; Liu, Z.; Liu, L.; Wang, X.; Su, X.; Ma, Q. A Novel Ultrasensitive Carboxymethyl Chitosan–Quantum Dot–Based Fluorescence “Turn On–Off” Nanosensor for Lysozyme Detection. *Biosens. Bioelectron.* **2014**, *61*, 9–13.

(49) Wang, J.; Wei, T.; Li, X.; Zhang, B.; Wang, J.; Huang, C.; Yuan, Q. Near–Infrared–Light–Mediated Imaging of Latent Fingerprints based on Molecular Recognition. *Angew. Chem., Int. Ed.* **2014**, *53*, 1616–1620.

(50) Tan, W.; Donovan, M. J.; Jiang, J. Aptamers from Cell–Based Selection for Bioanalytical Applications. *Chem. Rev.* **2013**, *113*, 2842–2862.

(51) Meng, H. M.; Fu, T.; Zhang, X. B.; Tan, W. Cell–SELEX–Based Aptamer–Conjugated Nanomaterials for Cancer Diagnosis and Therapy. *Natl. Sci. Rev.* **2015**, *2*, 71–84.

(52) Yuan, Q.; Wu, Y.; Wang, J.; Lu, D.; Zhao, Z.; Liu, T.; Zhang, X.; Tan, W. Targeted Bioimaging and Photodynamic Therapy Nanoplat-form Using an Aptamer–Guided G–Quadruplex DNA Carrier and Near–Infrared Light. *Angew. Chem., Int. Ed.* **2013**, *52*, 13965–13969.